

## IPM SYSTEMS FOR J-PARC RCS AND MR

K. Satou, S Lee, T. Toyama, KEK, Tsukuba, Japan  
H. Harada, N. Hayashi, A. Ueno, JAEA, Tokai, Japan

### Abstract

Residual gas Ionization Profile Monitors (IPMs) are used at the J-PARC RCS and MR. The IPM is one of the most promising nondestructive profile monitor. However, usage in the high power accelerator like J-PARC, whose beam intensity will overcome  $4E13$  particle per bunch, is challenging, because interferences with the space charge electric field of the intense beam should be carefully estimated.

The overview of the systems and the present statuses are described. The external electric field error of the RCS IPM, and the issue on contaminations on the electron collection mode are also discussed.

### INTRODUCTION

The residual gas Ionization Profile Monitors (IPMs) are employed in Rapid Cycling Synchrotron (RCS) and in Main Ring synchrotron (MR) of J-PARC. The IPM uses the charged particles generated by the interaction of beam with the residual gas in the vacuum chamber. The external electric field with high uniformity are required to project the particles across the beam to a detector which mounted on the horizontal and the vertical plane. The IPM is one of the most ideal diagnostics because it induces no beam loss.

However, due to its quite complicated collection process, collecting the charged particles in the strong space charge electric field by the intense beams, it needs cross checking with other profile monitors like Multi Wire Profile Monitor (MWPM). If the space charge electric field is weak, then the effect becomes negligible with increasing a high voltage for particle collection (HV). However, the maximum space charge electric field of the J-PARC beam will reach to that of the order of 1 MV/m depending on the bunching factor. The usage in such a high space charge electric field is challenging.

There are two mode operations, ion collection and electron collection. The usage of the ion collection mode in a high power synchrotron is reported in Ref. [1].

At present, the ion collection mode are mainly used at the RCS and the MR, however, with increasing the intensity of the beam, the electron collection with guiding magnetic field ( $B_g$ ) will be required [2]. As for the RCS, the electron collection mode with the  $B_g$  is also adopted.

After introducing the present IPM system, an issue on the particle collection error by the external electric field of the RCS IPM and large contaminations on the electron collection mode without the  $B_g$  measured at the MR IPM are presented.

### OVERVIEW OF THE SYSTEM

Schematic drawing of the horizontal IPM system is shown in Fig. 1.

In the RCS, two IPMs are installed to measure horizontal and vertical profile. The locations of the RCS IPMs are shown in Fig. 2. The horizontal IPM is at the arc section where the dispersion function is 3.9 m. The new IPM system will be installed in the straight section where the dispersion is zero. As for the MR, two IPM systems, horizontal and vertical, have been installed at the straight section where the dispersion is zero, and the new IPM system has installed during this summer shut down at the arc section where the dispersion is 2.1 m. This IPM is not yet operated. The locations of the MR IPMs are shown in Fig. 3.

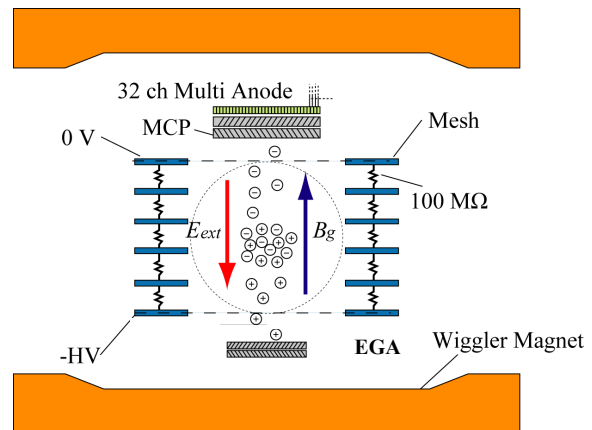


Figure 1: The schematic drawing of the IPM with magnet.

A set of the electrodes connected with the resistors is used to produce the external electric field to collect charged particles. The gap size of the electrodes is equal to the diameter of the beam window which is 297 mm for the RCS IPM and 130 mm for the MR IPM, respectively. The maximum HV for the RCS IPM and the MR IPM are 45 kV and 50 kV, respectively. By changing the polarity of the HV, both the positive ions and the electrons are collected. At present, the operating HV is limited to under 30 kV for the MR IPM to meet the internal criteria for electrical facilities. However, it will be upgraded sooner.

Rectangular chevron type microchannel plate (MCP) with multi strip anode is used for signal multiplication and signal read out. The active area of the MCP is  $81 \times 31 \text{ mm}^2$ . As for the RCS, the 3 MCPs are used to measure the large emittance beam of  $216 \pi \text{ mm mrad}$ . One 32ch multi-anode (anode width is 2.5 mm) type

MCP mounted at center are for a beam core measurement, and another two 8ch multi-anode (anode width is 10 mm) type MCPs are for a beam tail measurement. Details of the RCS IPM are given elsewhere [3]. As for the MR IPM, one 32ch multi-anode (anode width is 2.5 mm) type MCP is used.

To check the gain balance of the MCP, Electron Generator Array [4] is used as an electron checking source.

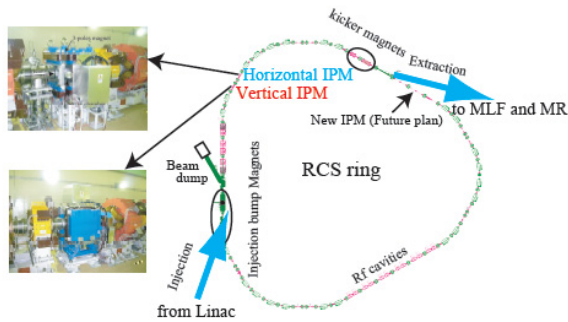


Figure 2: The locations of the 2 IPM systems in the RCS are shown. These systems are installed at arc section. The location of the new horizontal IPM is also.

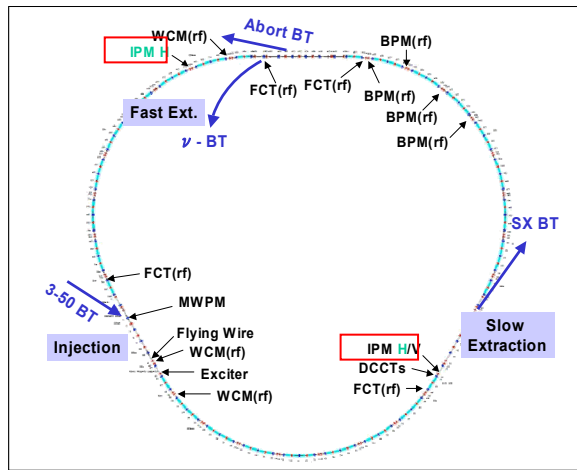


Figure 3: The locations of the IPM systems in the MR are shown.

### Magnet System for the RCS IPM

The 3-poles wiggler magnet was installed at the RCS IPM to generate guiding magnetic field ( $B_g$ ). The magnet was designed such that the line integral of the magnetic field along the beam axis is zero so as not to kick the circulating beam. Figure 4 shows the distributions of the magnetic fields. As can be seen in the figure, the calculated vertical field  $B_y$  well reproduces the measured one. The flatness of the  $B_y$  in the area of interest, that is the detector area, is 0.05 % along the horizontal axis and 2 % along the beam axis. The maximum  $B_y$  field at the center is 50 mT.

Besides a main coil, a sub coil is set to the center pole to tune the line integral of the  $B_y$  along the beam axis to completely zero. A Closed-Orbit Distortion (COD) by the residual dipole field excited by the main coil were measured at first, then the sub coil was excited to minimize the COD.

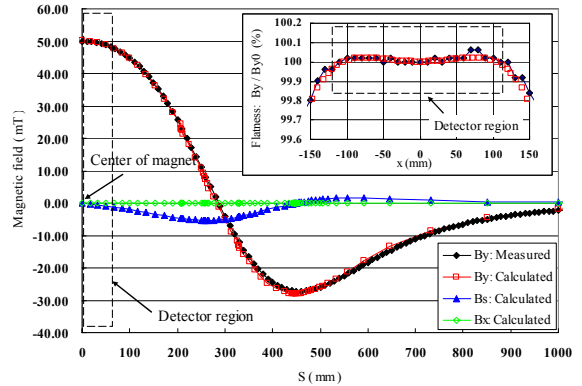


Figure 4: The measured vertical magnetic fields with the calculated ones. The  $B_y$ ,  $B_x$ , and  $B_s$  is the vertical field, the horizontal field, and the field along beam axis, respectively. The horizontal axis is the distance from magnet center (=IPM center) in unit of mm. The vertical axis is the field intensity in unit of mT. The flatness of the  $B_y$  field along horizontal axis on the cut plane at magnet center are also shown.

### Data Taking System

The block diagram of the data taking system is shown in Fig. 5. An output current from a MCP anode is input to an amplifier whose input impedance is 1 k $\Omega$ . The gain of the amplifier is selectable as 10, 100, and 1000. Since the typical cable length from the IPM to the amplifier is 30 m, the amplifier output shows an exponential decay like response to the delta function like input with the decay constant of 3  $\mu$ s which is the product of the input impedance and the input capacitance to the amplifier. Since the decay constant is smaller than the beam revolution of the RCS and the MR, turn by turn profiles can be measured, although some fraction is overlapped.

An output of the amplifier divided into two. One is processed by the oscilloscopes with the band width of 200 MHz and the maximum sampling speed of 200 MS/s. The resolution of the analog to digital conversion is 13 bit. The data length of each anode is 1M word. The SAD [5] based OPI software controls the oscilloscopes and displays the profiles.

A typical number of the collected charged particles at the MCP which corresponds to a single anode output is a several hundreds per one bunch beam per one passage, thus the statistical error is not negligible. Moreover the MCP is operated under the analog mode, the fluctuation of the gain is not negligible if the number of the detected particles is small. The averaging function of the oscilloscopes helps to reduce these errors and also to reduce random noise.

Another output is integrated during arbitrary time. The each output signals are processed by a multiplexer.

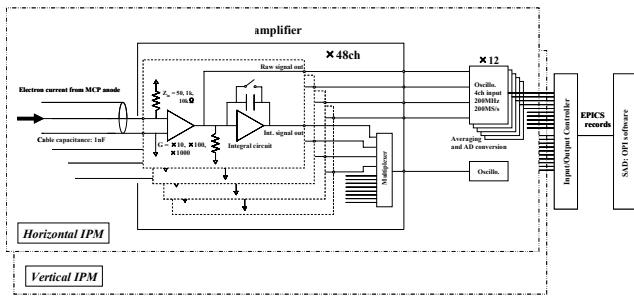


Figure 5: The block diagram of the data taking system.

*Consistency of the Beam Emittance between the IPM and MWPM*

To check the reliability of the IPM systems, the obtained root mean square (rms) emittances measured by using the MR-IPMs were compared with those measured by using the Multi-Wire Profile Monitors [6] installed in RCS to MR beam transport line (3-50BT), here the ions were used to obtain the profile. A one bunch beam with the intensity of 4.5E12 particle per bunch (ppb) and the bunching factor of 0.036 was injected to the MR through the 3-50BT and then extracted to the beam dump immediately after passing through the straight line section for Slow Extraction where the IPM systems are installed (single bunch one pass mode). The IPM systems then measured only one pass beam profile. The collection HV was 30 kV.

The measured horizontal and vertical rms emittances by using the IPM were 6.2 and 5.0  $\pi$  mm mrad respectively, and these by using the MWPM were 4.5 and 2.9  $\pi$  mm mrad respectively. The ratio of the beam size measured by using the IPM to that measured by using the MWPM is 1.2 for horizontal and 1.3 for vertical.

This inconsistency is likely to be due to the space charge effect of the beam. Since the space charge electric field acts as the repulsive force upon the positively charged ions on the way to the MCP detector, then the IPM shows broad beam profile. The inconsistency depends strongly on the collection HV and the space charge electric field. The quantitative study of the effect is reported in Ref. [7].

*Turn by Turn Profile Measurement*

To tune injection errors, turn by turn profile measurements are used. Figure 6 shows the measured profiles by the horizontal MR IPM, from 1<sup>st</sup> turn to 14<sup>th</sup> turn. Here, one bunch beam was injected. The IPM operated under the ion collection mode. The time separation between each profile is 5.2  $\mu$ s. The left hand side figure shows the profiles before injection error tuning. As can be seen in the figure, there are the dipole and quadrupole oscillations. The right hand figure shows the profiles after injection error tunings.

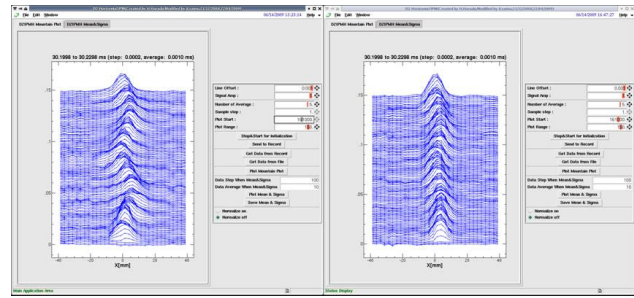


Figure 6: Mountain plot of turn by turn profiles in the MR from just after one bunch beam injection, measured before (left) and after (right) the injection tunings. The vertical axis shows time in arbitrary unit from downward to upward, and horizontal axis shows beam size in unit of mm.

**ISSUE ON THE EXTERNAL ELECTRIC FIELD OF THE RCS IPM**

The present external electric field of the RCS IPM is distorted, and the measured beam profile is shrunk to a half. The left hand side of the Fig. 7 shows the present IPM model for 3D field calculation and the calculated potential map on the cut plane of the IPM center which is perpendicular to the beam axis, here the 3D calculation code, CST studio suite [8] was used.

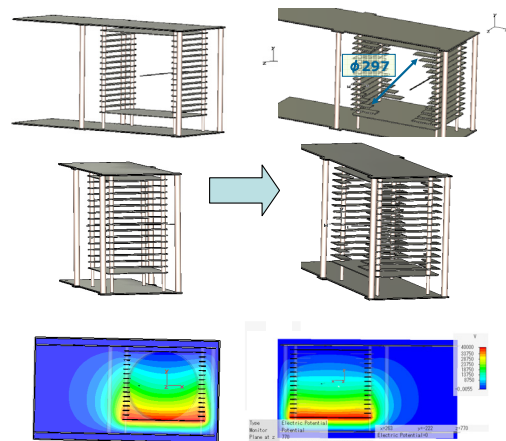


Figure 7: The left figures are the present RCS IPM model and the calculated potential map on the cut plane at IPM center which is perpendicular to the beam axis. The right figures are that of the recovery plan.

The calculations suggest that the Ex and Es cannot be negligible, where Ex, Ey and Es is electric field along horizontal axis, vertical axis, and beam axis, respectively. The Ex and Es induce the profile distortion for the case of the ion collection mode.

To obtain the calibration curve, the local bump orbit was used. The beam positions from the IPM were compared with the beam positions measured by the beam position monitors (BPMs). The HV was 45 kV.

The 3D particle tracking calculations using CST studio suite was made. Figure 8 shows the measured and calculated results. The black solid line with black solid circles shows the calculated results. The calculation suggests:

$$P_{IPM} = 0.5 \times P_{Beam},$$

where  $P_{IPM}$  is a beam position from IPM and the  $P_{Beam}$  is a beam position. As can be seen in the figure, the calculations reproduce well the experimental data within  $-70 \text{ mm} \sim +70 \text{ mm}$ . By using the model, the beam emittance is estimated.

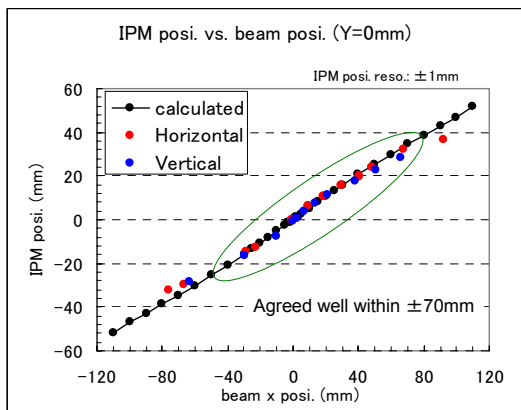


Figure 8: The figure shows the response of the RCS IPM. The horizontal axis shows the beam position from the BPMs and the vertical axis shows the beam position from the RCS IPM. The red and blue solid circles are the experimental data, horizontal and vertical, respectively.

As for the electron collection mode with the  $B_g$ , the  $E_s$  makes the cross term force with the  $B_g$ , and its force also makes the profile distortion. Note that the center MCP is mounted at  $s=s_0+45 \text{ mm}$  and the side MCPs are mounted at  $s=s_0-45 \text{ mm}$ , where the  $s_0$  is the center coordinate of the IPM along the beam axis, so as to overlap each other as shown in Fig. 2 of Ref. [3]. To obtain the profile by the electron collection mode using the  $B_g$ , improvements of the uniformity of the external electric field are required.

The field can be recovered by optimizing the shape of the electrodes as shown in the right side of the Fig. 7 and HV balance to each electrode by tuning the resistors. The calculated potential map shows improved field. The calculated field suggests that the good area for particle detection is only  $s_0 \pm 10 \text{ mm}$  along the beam axis. The modification of the MCP arrangement is also required.

### THE ISSUE ON THE DELAYED AND LARGE NEGATIVE CHARGE SIGNALS ON THE ELECTRON COLLECTION MODE

The most serious issue on the electron collection mode is whether the IPM can collect only the detached electrons by the beam interaction with residual gas.

From present gas pressure in the IPM chamber of the order of  $10^{-6} \text{ Pa}$  and the beam intensity of  $0.5E13 \text{ ppb}$ , the number of the incoming electrons to the MCP detector is a several thousand per one bunch per one passage. This small number of the detected electrons means that the obtained beam profile is very sensitive to the electrons from other processes induced by the beam; discharge electrons from the HV electrodes inside the IPM chamber, electron emission from a surface of the EGA induced by the positive ions which is move backward to the EGA, electrons from outside chamber of the IPM chamber. Unfortunately, at present, we can not apply the electron suppression voltage to the mesh plate in front of the EGA. The last electrons will be induced by the beam loss and gas ionization and will be triggers of the e clouds generation which involves the electron multiplication.

To check the effect of the undesirable electrons, we compared the 2 profiles by the two mode operations measured by using the MR IPMs. Note that the MR IPMs have no  $B_g$ . We used the single bunch one pass mode operation, where the beam intensity and the bunching factor was  $4.5E12 \text{ ppb}$  and  $0.036$ , respectively. The HV for the electron collection was limited under  $15 \text{ kV}$  because the HV generator whose current limit is  $7.5 \text{ mA}$  was down due to the over current error. On the other hand, there is no over current error for the ion collection. The MCP bias was fixed to check directory the signal intensities between the two modes. We changed the MCP bias setting and check waveforms to ensure that the MCP is operated without gain degradation due to large output current.

Figure 9 shows output signal from the MCP anode, each is the averaged waveform of every 4ch out of the 32ch anodes in total. The average of all signals is also shown. As can be seen in the figure, the integrated output signals of the electron collection mode (right figure) is about 10 times larger when compared to that of the ion collection mode (left figure). Each HVs were  $15 \text{ kV}$ .

Taking into account the detection efficiency of the MCP which is  $60 - 85 \%$  for positive ions and about  $20 \%$  for electrons for the kinetic energy range of interest, around  $7.5 \text{ kV}$ , the number of the detected electrons is  $30 \sim 45$  times larger than that of positive ions. This means that the main partial of the output signal of the electron collection mode is not due to the detached electrons. Note that the detection efficiency is depends also on the kinetic energy of the charged particles, thus we cannot clearly say that the ratio is just the ratio of the number of the detected particles. If we assume that the almost all the detected particles are electrons whose kinetic energy is from  $0.2 \text{ kV}$  to  $20 \text{ kV}$ , where the detection efficiency is vary from  $20$  to  $85 \%$ , the ratio of the detected number of the electrons to the positive charged ions is thus  $7$  to  $45$ . There is also a possibility of contamination of the negative charge ions.

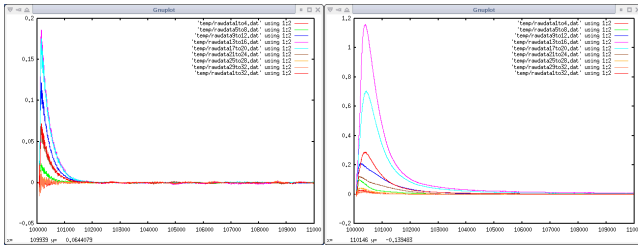


Figure 9: The output waveforms for the ion collection mode (left) and the electron collection mode (right). The horizontal axis shows the time in unit of 10ns. The full scale of the horizontal axis is  $100 \mu s$ .

The waveforms of the electron collection mode shows the main component of the negative charged particles is detected delayed after about  $3 \mu s$  from the beam passage. The time of flight (TOF) of the electron from the IPM center to the detector is  $3.5 ns$ , on the other hand, that of the ion is  $0.2 \mu s$  in typically. This fact suggests that the main component of the signal is not due to the electrons from EGA because it takes sum of the TOF of positive ion from ionization point to the EGA and the TOF of secondary electrons from EGA to MCP. Therefore the electrons will reach on the MCP surface at nearly the same time as positive ions.

Figure 10 shows the mountain plot of the profile measured for the electron collection mode. The arrow in the figure shows the beam position,  $6.2 mm$ , obtained by the BPMs. The extracted beam position from the profile measured by the ion collection mode is  $6.9 \pm 0.2 mm$  and this value is agreed well with the beam position from the BPMs considering that the present anode width is  $2.5 mm$ . On the other hands, as can be seen in the figure, the profile center is shifted to the center and the shape becomes narrow with increasing the time.

These facts clearly show that the detected particles on the electron collection mode have large contaminations from other processes. To clear the source, more theoretical and experimental studies are needed.

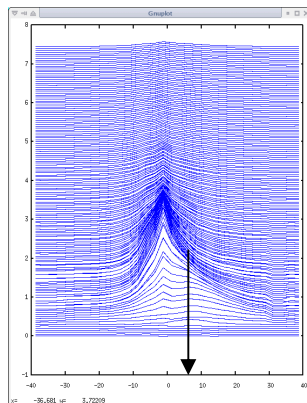


Figure10: The mountain plot of the measured profile. Horizontal axis shows the size of profile in unit of mm and the vertical axis shows time in arbitrary unit. The full scale of the vertical axis corresponds to  $22.5 \mu s$ . Solid arrow shows beam position measured by BPMs.

## SUMMARY AND CONCLUSION

The IPM systems were developed and used at the J-PARC RCS and MR. The overview of the system was described.

These systems are now mainly operated under the ion collection mode. The measured turn by turn profiles show clear contributions from the dipole and the quadrupole oscillations by injection errors, and these are used for the injection tunings. However, the mode is vulnerable to the space charge electric field of the circulating beams. The inconsistencies of the measured beam size between the IPM and the MWPM are likely to reveal the effect. The beam size from the IPM is larger than that from the MWPM by 20 % to 30 %. The effect will be more serious with increasing the beam intensity in the future. The present IPM systems require improvements to measure the beam in good resolution.

As for the RCS, the profile is shrunk to a half by the external electric field distortion. The beam based calibration assisted with the 3D field and particle tracking calculations is now adopted. The recovery of the field error will be possible by changing the shape of the electrodes and by optimizing the HV on each electrode.

Usage of the IPM in such an intense space charge electric field requires the electron collection mode with the Bg. The RCS IPM has the 3-poles wiggler magnet system, however, due to the inhomogeneous external electric field, the profile is distorted. Moreover, large contaminations were measured at the MR IPM using electron collection mode without Bg. Sources of the contaminations is now unclear. More detail experimental and theoretical studies are needed because the contaminations will limit the resolution of profile measurement using the electron collection mode with and without the Bg.

## REFERENCES

- [1] B. G. Pine et al., EPAC06, p 1082, (2006), S. J. Payne et al., DIPAC07, p 364, (2007), S. A. Whitehead et al., BIW10, (2010).
- [2] P. Cameron et al., PAC99, p. 2114 (1999), R. Connolly et al., PAC01, p. 1297 (2001), J. R. Zagel et al., PAC01, p. 1303 (2001), G. Ferioli et al., DIPAC03, p.116 (2003), C. Fisher et al.,BIW04, p. 133 (2004).
- [3] K. Satou et al., EPAC08, p. 1276, (2008).
- [4] Electron generator array is a cold electron source using MCP produced by the PHOTONIS Ltd.
- [5] Computer program complex for accelerator design. See <http://acc-physics.kek.jp/SAD/>
- [6] Y. Hashimoto et al., these proceedings.
- [7] K. Satou et al., EPAC06, p. 1163, (2006).
- [8] The program complex using the finite integration technique, which includes electric and magnetic 3D field calculator and particle tracking in 3D.